NJC

Accepted Manuscript

This is an *Accepted Manuscript*, which has been through the Royal Society of Chemistry peer review process and has been accepted for publication.

Accepted Manuscripts are published online shortly after acceptance, before technical editing, formatting and proof reading. Using this free service, authors can make their results available to the community, in citable form, before we publish the edited article. We will replace this *Accepted Manuscript* with the edited and formatted *Advance Article* as soon as it is available.

You can find more information about *Accepted Manuscripts* in the Information for Authors.

Please note that technical editing may introduce minor changes to the text and/or graphics, which may alter content. The journal's standard Terms & Conditions and the Ethical guidelines still apply. In no event shall the Royal Society of Chemistry be held responsible for any errors or omissions in this *Accepted Manuscript* or any consequences arising from the use of any information it contains.

ROYAL SOCIETY OF CHEMISTRY

www.rsc.org/njc

Cite this: DOI: 10.1039/c0xx00000x

www.rsc.org/xxxxxx

ARTICLE TYPE

Gold nanoparticle-mesoporous silica sheet composite with enhanced antibody adsorption capacity

Kazuma Nakanishi,[a,b] Masahiro Tomita,[a] Yoshitake Masuda[b] and Katsuya Kato*[b]

Received (in XXX, XXX) Xth XXXXXXXXX 20XX, Accepted Xth XXXXXXXXX 20XX

DOI: 10.1039/b000000x

A notably high-capacity antibody adsorbent was demonstrated using dispersed gold nanoparticles immobilised on a mesoporous silica sheet. The mesoporous silica sheet (MPS sheet) was prepared *via* a dual-templating method using tetraethoxysilane and 3-aminopropyltriethoxysilane as the silica framework materials. Gold nanoparticles were loaded on the amino-functionalised surface of the MPS sheet *via* deposition–precipitation using $HAuCl_4$ as the Au colloid precursor and then crystallised *via* calcination. The properties of the gold nanoparticle-silica composite and the dispersion of the nanoparticles were characterised using transmission electron microscopy, energy-dispersive X-ray spectroscopy and X-ray diffraction analyses. The surface characteristics of gold nanoparticle composite materials calcined at different temperatures were also evaluated using Fourier transform-infrared spectra, X-ray photoelectron spectroscopy and thermogravimetry data. The mesoporous silica-gold nanoparticle composite sheet crystallised at 550 °C (sheet-Au-550) was mesoporous in character (pore diameter = 3.8 nm) with a BET surface area of 258.0 m^2g^{-1}. With respect to antibody adsorption, the sheet materials had a relatively higher capacity than the typical cylindrical mesoporous silica, and sheet-Au-550 exhibited strong performance (maxim adsorption quantity Q_{Max} = 0.26 mg IgG/mg carrier). In addition, the IgG adsorption equilibrium for sheet-Au-550 fit the Langmuir isotherm model better than the Freundlich plot model. These results will be very useful for the design of adsorption materials for biomolecules, such as antibodies.

Introduction

Antibodies are immune-system biomolecules produced by B cells *in vivo*. Immunoglobulin G (IgG) is a typical isotype antibody with a molecular weight of approximately 150 kDa and an isoelectric point of 5.0 to 9.5. Antibodies have been immobilised on a wide variety of solid materials for practical applications, including in immunoassays, nanomedicine, detection and separation.[1–4] Nano-shells, polymers, porous materials, agarose and gold nanorods have all been used as IgG adsorbents.[5–7] For the immobilisation of IgG on an adsorbent, it is known that chemical binding is useful, particularly in Fab region-specific binding (an antigen-antibody complex reaction).[8,9] Previously, the specific binding of IgG and protein A (antigen) was applied for highly efficient affinity column chromatography purification of IgG.[10] For efficient IgG immobilisation, surface functionalisation on the adsorbent was attempted using various chemistries, including amino, thiol, carboxyl and epoxy groups.[11,12]

Porous materials are of great interest because their pore structures can interact with various species, including atoms, ions, molecules and nanoparticles; as a result, they can be used in adsorption/separation, catalytic and sensing applications. Since the discovery of mesoporous silica (MPS) by Kuroda *et al.* in 1990, synthetic developments and applications of MPS have received much attention.[13,14] MCM-41, which has a typical two-dimensional hexagonal structure of cylindrical mesopores, was developed by Mobil researchers as part of the M41S family.[15] For its preparation, long-chain alkyltrimethylammonium halides (ion surfactants) were used as structure-directing agents. These surfactants form a lyotropic liquid-crystalline phase, leading to the self-assembly of silica frameworks *via* condensation of silica oligomers. The porous structure was obtained by the removal of surfactant *via* calcination or extraction. MPS materials have been prepared with various structures, including three-dimensional hexagonal, cubic and spherical shapes. Notably, MPS can be further functionalised to enhance its ability to interact with other species and to increase its practical utility, such as *via* organic or magnetic functionalisation.[16–18]

Colloidal gold has been widely used in immunoassays and as an efficient carrier for biomaterials that have relatively large surface areas and is known for its easy preparation, good biocompatibility and enhancement of electron-transfer kinetics.[19–23] A colloidal gold layer not only increases the quantity of immobilised antibodies, but also preserves the specific activity of the biomolecules. Researchers have also demonstrated improvement of antibody-antigen immunosensor sensitivity using colloidal Au.[24] Antibody-immobilised silica-coated gold nanorods and nano-shells have also been applied to biomedical applications.[25,26] Biofunctionalisation of proper gold nanoparticles has also been

shown to have a positive impact on applications that rely on antibodies.[27]

Previously, we investigated the preparation and application of MPS sheets. The sheet structure was designed using dual-templating with *N*-palmitoyl-L-alanine and triblock copolymer P123. These two surfactants played a role in determining the sheet framework, while tetraethoxysilane (TEOS) and 3-aminopropyltriethoxysilane (APTES) as the silica sources also influenced the silica structural morphology. Enzymes immobilised on the MPS sheet exhibited improved catalytic activity.[28] In addition, the MPS sheet had a high capacity for the adsorption of metal ions.[29] These results indicated that MPS sheets have the potential to be highly effective adsorbents.

The enhancement of antibody adsorption materials is a great necessity because antibodies are commonly used in biochemistry, molecular biology and medical research and for immunoassays and affinity column chromatography. In the present study, therefore, the MPS sheet was applied as a large-quantity antibody adsorption material. In addition, to enhance the adsorption of IgG, Au nanoparticles (AuNPs) were first loaded on the MPS sheet. Generally, it is difficult to load gold onto silica materials *via* deposition–precipitation using $HAuCl_4$ as the Au colloid precursor because silica surfaces are highly negatively charged.[30] Commonly used synthetic strategies to overcome this issue include stabilisation of the colloidal gold nanoparticles *via* binding with an organo-functionalised silane as a ligand or immobilisation of AuNPs in an organic polymer matrix.[31–37] In particular, Lee *et al.* reported that amino-functional ligands successfully enabled the loading of AuNPs on a supported MPS surface.[38,39] Thus, an MPS sheet with surface aminopropyl groups (sheet-NH_2) was prepared using the original co-condensation method. To investigate the material structure and surface functionalisation, a calcined MPS sheet (sheet-cal), typical MCM-type MPS (MCM-NH_2) and a non-porous spherical silica material (Stöber-NH_2) were synthesised. Subsequently, AuNPs were loaded onto each material *via* the surface amino-functionalised ligands. The IgG adsorption capacity for each material was then determined, and the adsorption kinetics were evaluated using the Langmuir and Freundlich isotherm plot models and the resultant sorption equilibriums.

To the best of our knowledge, there have been no previous reports of MPS sheet-AuNP composite materials for biomolecule capture applications. It was found that the IgG adsorption capacity of the composite was dramatically increased over that of MPS due to the combination of its optimal adsorbent structure and the presence of the AuNPs on the support. These results will enable the development of new antibody adsorption materials.

Experimental

Materials

Palmitoyl chloride, L-alanine, cetyltrimethylammonium chloride (CTAC), acetone, 28% ammonia solution, sodium hydroxide, hydrogen tetrachloroaurate (III) tetrahydrate and hydrochloric acid were purchased from Wako Pure Chemical Industries, Japan. Triblock copolymer Pluronic P123 ($EO_{20}PO_{70}EO_{20}$; Mn ca. 5800 g mol^{-1}) and immunoglobulin G (IgG) from human serum were obtained from Sigma-Aldrich, St Louis, MO. Bio-Rad protein assay dye reagent concentrate (Cat # 500-0006) was purchased from BIO-RAD, Hercules, CA. TEOS and APTES were obtained from Shin-Etsu Chemical Co., Japan. All other chemicals were analytical grade and used without further purification.

Preparation of silica materials

The MPS sheet was prepared according to our previous reports.[28,29] The sheet-structured silica was synthesised using TEOS and APTES as silica sources *via* a dual-templating synthetic process. The resulting silica was refluxed in ethanol (200 mL) for 2 days in order to remove the templates without eliminating the aminopropyl groups from the APTES. The synthesised sheet-NH_2 was washed with water and ethanol and collected *via* centrifugation. In addition, a sheet-cal sample was prepared by calcining the sheet-NH_2 material at 500 °C to remove the organic templates.

MCM-type mesoporous silica was also synthesised using CTAC (2.6 g) as the template. A similar molar ratio of TEOS (1.46 g) to APTES (0.28 g) as used for the MPS sheet preparation was added to the dissolved organic template solution (pH = 0.5 with HCl). After stirring for 5 h, ammonia (14.7 M, 3.0 mL) was added to the reaction mixture, and the mixture was stirred for another 24 h. The resulting precipitate was collected *via* centrifugation at 6000 rpm, washed repeatedly with water and then refluxed for 2 days in a mixture of ethanol (200 mL) and conc. HCl (2 mL) in order to remove the template. The MCM-NH_2 was collected *via* centrifugation and then washed with water, ethanol and acetone to dryness.

The spherical silica material was synthesised according to Stöber's method.[40] Deionized water (17.7 g), methanol (175 mL) and a 28% aqueous ammonia solution (7.2 g) were mixed together. TEOS (1.46 g) and APTES (0.28 g) were then added to the mixture. After 3 s of stirring, the mixture was aged at 25 °C for 20 h. The resulting Stöber-NH_2 was washed with water and ethanol and then centrifuged at 6000 rpm with acetone.

Synthesis of gold nanoparticles supported on the silica materials

Each silica material (sheet-NH_2, MCM-NH_2 and Stöber-NH_2, 100 mg) was added to a separate 3×10^{-4} M $HAuCl_4 \bullet 4H_2O$ ethanol solution (10 mL). The mixtures were sonicated for 1 h in order to introduce the gold precursor into the mesopores. The resulting materials were collected *via* centrifugation, vacuum dried at room temperature for 6 h and then calcined in a muffle furnace at 550 °C. The heating rate was 1 °C/min, and each solid was calcined for 1 h.

Adsorption of immunoglobulin G by the silica materials

First, IgG from human serum was dissolved in a 10 mM phosphate buffer (pH = 7.0). The IgG solution (1.0 mL; 0.1 to 0.7 mg/mL) was then added to each of the synthesised silica materials. Each suspension was stirred for 3 h at 25 °C to allow adsorption of the IgG on the carrier materials. The supernatants were then separated from the solid precipitates *via* centrifugation

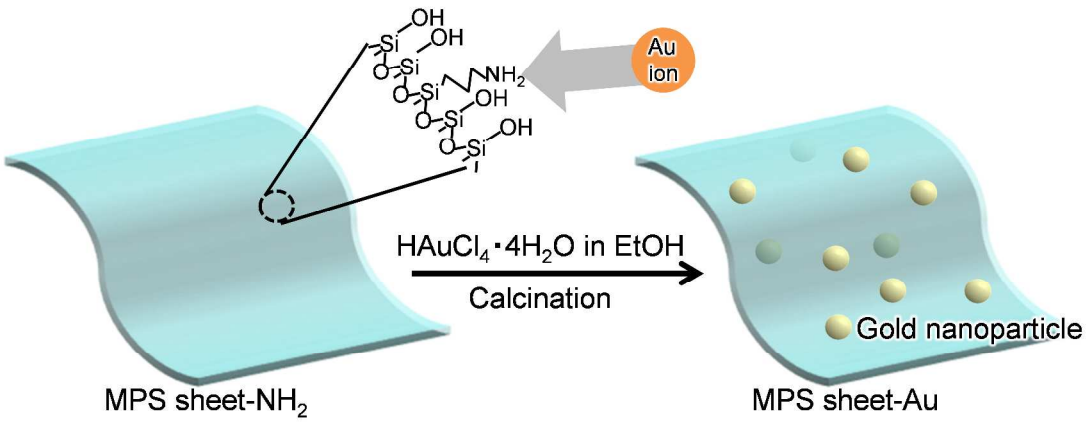

Scheme 1 Schematic representation of synthetic procedure of MPS-sheet-Au composite for antibody adsorbent.

at 12000 rpm and 4 °C. The IgG concentration was determined using the Bradford method and a Bio-Rad protein assay dye reagent.[41] The quantity of adsorbed IgG on each silica material was calculated from the quantity of IgG remaining in the supernatant. All of the reported data are the averages of the results obtained for at least four adsorption experiments.

Adsorption isotherm modelling

The equation for the Langmuir isotherm plot model is

$$q_e = \frac{q_m k_L C}{1+k_L C},$$

where q_e (mol/g) is the quantity of IgG adsorbed on the silica material at adsorption equilibrium, q_m (mol/g) is the quantity of adsorbate adsorbed per unit mass of adsorbate corresponding to complete monolayer coverage, k_L (L/mol) is the Langmuir isotherm constant and C (mol/L) is the equilibrium IgG concentration in solution. The equation can be reformulated as follows:

$$C/q_e = C/q_m + 1/q_m k_L.$$

The values for q_m and k can be calculated from the slope and intercept, respectively, of the linear plot of C/q_e versus C.

The Freundlich isotherm plot model equation is

$$q_e = k_F C^{1/n},$$

where k_F (L/g) is the Freundlich constant indicating the adsorption capacity and *1/n* is a constant related to the sorption intensity. A linear form of the equation can be given as follows:

$$\ln q_e = \ln k_F + \frac{1}{n}\ln C.$$

The values for k_F and *1/n* were determined from the intercept and slope, respectively, of the linear plot of ln q_e vs. ln C.

Characterisation

To characterise the morphology of the prepared samples, a field emission scanning electron microscope (FE-SEM, S4300, Hitachi, Japan) operated at an accelerating voltage of 10 kV and a transmission electron microscope (TEM, JEM 2010, JEOL, Japan) operated at 200 kV were used. X-ray diffraction (XRD) patterns were obtained on a RINT2100V/PC (Rigaku, Japan) using Fe-Kα radiation operated at 40 kV and 30 mA. The Brunauer–Emmett–Teller (BET) specific surface areas and pore volumes of the samples were determined using nitrogen adsorption–desorption isotherms, and the pore size distribution curves were acquired using the Barret–Joyner–Halenda (BJH) method on a Micromeritics analyser TriStar 3000 (Shimadzu, Japan). Zeta potentials in deionized H_2O were determined using an ELS-Z zeta potential and particle size analyser (Otsuka Electronics Co., Japan). Fourier transform-infrared spectra (FT-IR) were obtained using an MFT-2000 (JASCO Co., Japan) with KBr pellets (sample/KBr = 1/99). X-ray photoelectron spectroscopy (XPS) was performed using an ESCA-3400 (Kratos analytical, Shimadzu, Japan). The x-ray source (MgKα, 1253.6 eV) was operated at 10 kV and 20 mA. Analysis of the Au ions was performed *via* inductively coupled plasma-optical emission spectrometry (ICP-OES) using an IRIS Advantage instrument (Nippon Jarrell-Ash, Japan).

Results and Discussion

Characterisation of the Au nanoparticle-supported silica materials

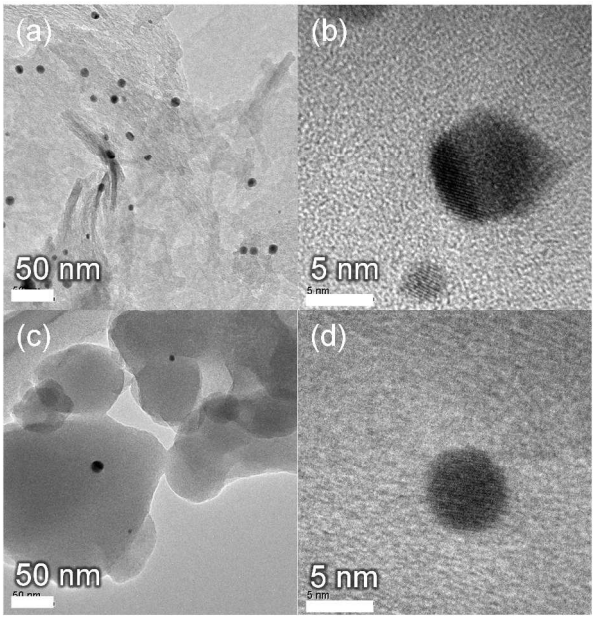

Fig. 1 TEM images of sheet-Au-550 [(a) × 50k, (b) × 800k] and MCM-Au-550 [(c) × 50k, (d) × 800k].

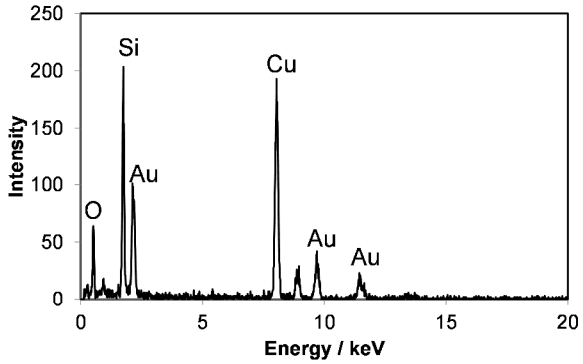

Fig. 2 EDX spectrum of the surface of sheet-Au-550 (from Fig. 1b).

The MPS sheets were prepared *via* a dual-templating approach using *N*-palmitoyl-L-alanine and Pluronic P123. The silane coupling agents TEOS and APTES were used as silica sources for the silica frameworks.[28,29] For comparison purposes, conventional cylindrical MCM-type MPS and a non-porous spherical silica material were also prepared using similar silica framework-forming conditions as were employed for the MPS sheets. Aminopropyl groups were introduced on the surfaces of all of the silica materials *via* the removal of the organic templates with ethanol extraction. Synthetic procedure of MPS-sheet-Au composite is illustrated in Scheme 1. Gold nanoparticles (AuNP) were then loaded on the prepared silicas *via* binding to the amino groups. Calcination at 550 °C was then performed to crystallise the nanoparticles. Note that sample name indicates the calcination temperature.

TEM images of the AuNP–silica material composites (sheet-Au-550, sheet-Au-200, MCM-Au-550 and MCM-Au-200) are shown in figure 1. From these images, it can be clearly seen that the AuNPs were loaded on an each silica material with good dispersion. In addition, the particle size distributions for the sheet-Au-550 samples were narrow, ranging from 7.0–10.5 (Fig. S1).The other AuNP-loaded silica materials exhibited similar tendencies. In fig. 1(b), clear Au (111) lattice fringes (d = 0.21 nm) can be seen in the TEM image of the sheet-Au-550. Similar lattice fringes were observed in the TEM images of the MCM-Au-550 sample (Fig. 1d). These results indicated that the AuNPs were highly crystallised at 550 °C calcination.

Figure 2 presents the EDX spectrum of the sheet-Au-550 sample shown in Figure 1b. Obvious Au peaks at 2.1, 9.7 and 11.5 keV can be seen in the spectrum. The EDX spectra of the MCM-Au-550 sample shown in Fig. 1d also contained similar peaks.

The spherical silica material (Stöber-silica) prepared using the Stöber method had a particle diameter of approximately 50 nm (Fig. S2). The AuNPs were also clearly loaded on this Stöber-silica, according to the TEM analysis (Fig. S3).

Figure 3 shows FE-SEM images of the sheet-Au-550 and MCM-Au-550 samples. In Figs. 3a, a sheet structure with a thickness of approximately 50 nm and a width of 1–2 μm can be seen. The MCM-type AuNP composite materials had polyhedral structures with particle sizes ranging from 200 to 500 nm (Fig. 3b). These FE-SEM analyses suggested that no structural changes in the silica occurred during the AuNP loading process.

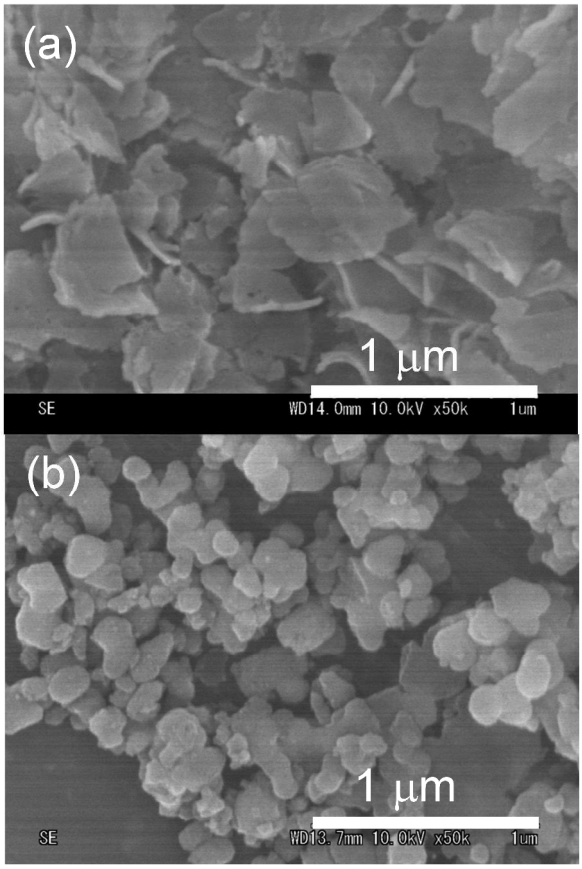

Fig. 3 FE-SEM images of (a) sheet-Au-550 and (b) MCM-Au-550.

Table 1 N_2 physisorption parameters and zeta potential of MPS materials and their gold nanoparticle composites.

Silica	Pore size (nm)[a]	Pore volume (cm^3g^{-1})[a]	Surface area (m^2g^{-1})[a]	Zeta potential (mV)[b]
Sheet-cal	3.8	0.47	190.0	–30.7
Sheet-NH_2	3.1	0.73	156.6	9.7
MCM-NH_2	2.7	0.39	302.5	10.5
Stöber-NH_2	-	-	84.3	4.7
Sheet-Au-550	3.8	0.59	258.0	–30.5
MCM-Au-550	2.6	0.59	576.4	–32.1
Stöber-Au-550	-	-	-	–33.1

[a]The BET surface area, pore volume and pore size distribution curves were obtained from the nitrogen adsorption–desorption isotherms using the BJH method.
[b]Zeta potential of MPSs (suspended in deionised water) was determined by zeta potential and particle size analyser ELS-Z.

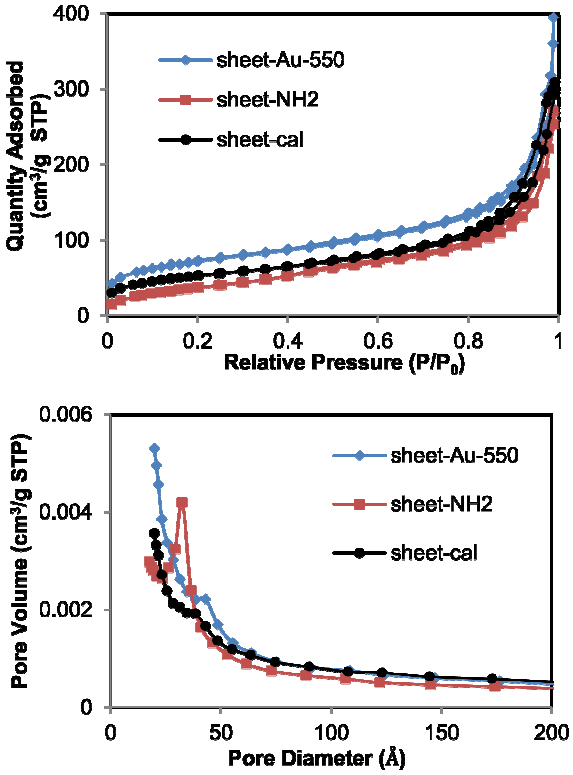

Fig. 4 Nitrogen adsorption–desorption isotherms and pore distributions for sheet-NH_2 (red) and sheet-Au-550 (blue).

Figure 4 shows the nitrogen adsorption–desorption isotherms and pore size distributions for sheet-NH_2 and sheet-Au-550. Each sheet material exhibited type IV sorption isotherms and type H3 hysteresis loops. Notably, in the pore size distribution plots, it can be seen that the higher calcination temperature resulted in narrower peaks and a shift to larger

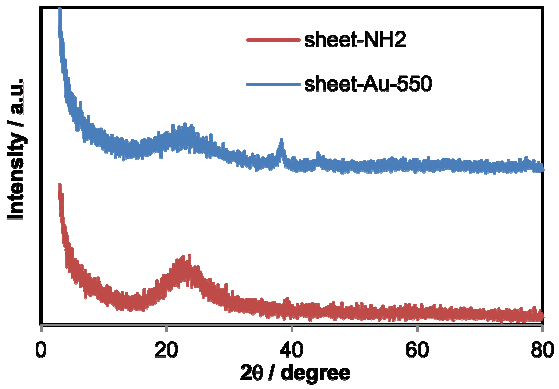

Fig. 5 XRD patterns of sheet-NH_2 (red) and sheet-Au-550 (blue).

diameters. The N_2 adsorption–desorption isotherms and pore size distributions for MCM-NH_2 and MCM-Au-550 are presented in Fig. S4. The physicochemical properties derived from the BET and BJH methods are summarized in Table 1.

The pore sizes for sheet-cal, sheet-NH_2 and sheet-Au-550 were 3.8, 3.1 and 3.8 nm, respectively, while the pore diameters for MCM-NH_2 and MCM-Au-550 were smaller at 2.7 and 2.6 nm, respectively. The specific surface areas of sheet-NH_2, sheet-Au-550, MCM-NH_2 and MCM-Au-550 were 156.6, 258.0 and 576.4 m^2g^{-1}, respectively. The zeta potentials of the materials are also listed in Table 1 and were found to be –30.5, –32.1 and –33.1 mV for sheet-Au-550, MCM-Au-550 and Stöber-Au-550, respectively. These results indicated that calcination at 550 °C led to materials with a higher negative charge than amino-functionalised silica materials, due to remove the surface aminopropyl group.

The structural characteristics of the samples were analysed *via* powder XRD. In Fig. 5, the XRD spectrum for sheet-Au-550 shows diffraction peaks at 2θ = 23° corresponding to amorphous

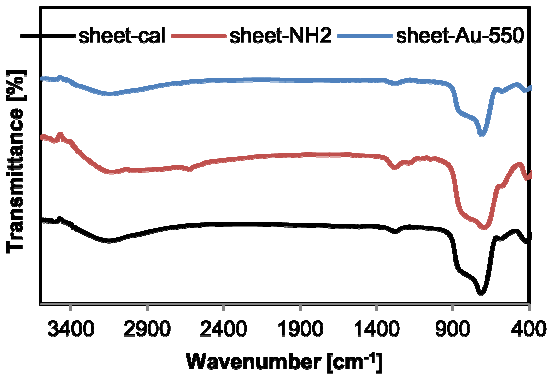

Fig. 6 FT-IR spectrum of sheet-cal (black), sheet-NH_2 (red) and sheet-Au-550 (blue).

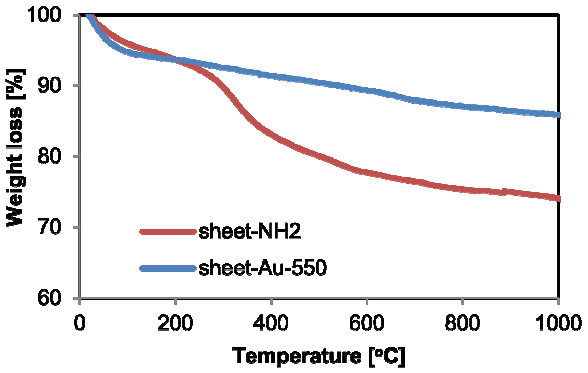

Fig. 7 Thermogravimetry (TG) curves for sheet-NH_2 (red) and sheet-Au-550 (blue).

silica and 2θ = 38°, 44° and 65° corresponding to metallic gold (111), (200) and (311), respectively. Similar XRD patterns for metallic gold were observed in the spectra for the MCM-Au-550 and Stöber-Au-550 (Fig. S5). The face-centred cubic lattice results for Au matched well with the lattice fringe lengths observed in the TEM images.

Analysis of the chemical states and compositions of the samples was also achieved using XPS (Fig. S6). No Au 4f and 4p peaks were detected, indicating the absence of AuNPs on the surfaces of the materials and suggesting that most of the AuNPs were loaded into the silica frameworks because of the adsorption of the Au colloid precursor (ionised Au) *via* deposition–precipitation into the interior of the porous silica followed by crystallisation.

Conversely, N 1s and Si 2p XPS peaks were observed, and the spectra for sheet-NH_2 indicated the presence of amino groups (Fig. S6b).

The FT-IR spectra of the sheet materials are shown in Fig. 6. All of the spectra included absorption bands for silanol groups (950 cm^{-1}) and silica vibrations (1080 cm^{-1}). The spectra for sheet-NH_2 also included C–H stretching bands at 2925 cm^{-1} corresponding to surface aminopropyl groups.

The TG curves for sheet-NH_2 and sheet-Au-550 are shown in Fig. 7. Sheet-NH_2 underwent significant weight losses between 200 °C and 500 °C attributed to the loss of aminopropyl groups; the weight losses for each were calculated to be 4.4×10^{-3} mmol/mg. The weight losses for the MCM-NH_2 and Stöber-NH_2 were determined to be 1.6×10^{-2} and 8.6×10^{-3} mmol/mg, respectively (Fig. S7). For all of the samples calcined at 550 °C, no sharp exothermic peaks were observed in the DTA curves. Based on the results of the TG and BET specific surface area analyses, it was concluded that a similar quantity of organic chains were present on the surfaces of the sheet-NH_2, MCM-NH_2 and Stöber-NH_2 samples.

Immunoglobulin G adsorption by the silica materials

The effects of the silica structure, surface aminopropyl groups and gold nanoparticles on IgG adsorption of the various materials were investigated. In these experiments, IgG was adsorbed on all of the prepared materials using equal amounts of an IgG solution (500 μg IgG/800 mL phosphate buffer). The quantities of adsorbed IgG are listed in Table 2. The sheet-Au-550 sample showed the best performance (0.26 mg IgG/mg silica), followed by the sheet-cal sample (0.21 mg/mg). The AuNP composite materials calcined at 550 °C adsorbed higher IgG quantities than the other samples. For example, MCM-Au-550 adsorbed 0.13 mg/mg IgG compared to 0.04 mg/mg for MCM-NH_2. From a different perspective, the surface amino-functionalised materials exhibited lower IgG adsorption capacities. The surfaces of these functionalised materials were more positively charged because of the presence of the surface amino groups, resulting in electric repulsion between the IgG molecules and the surface and consequently decreased adsorption compared to the non-functionalised silica samples. The specific surface area of AuNP composite materials was increased. These results indicated that the use of AuNP composite materials observed positive effect for IgG adsorption.

Next the adsorption isotherms for sheet-NH_2, sheet-cal, sheet-Au-550, MCM-Au-550 and Stöber-Au-550 were plotted (Fig. 8), and the maximum IgG adsorption quantities (Q_{Max}) for each sample were estimated from the isotherms (Table 2). The sheet-Au-550 sample exhibited a significantly high Q_{Max} of 0.26 mg/mg. The Q_{Max} values for sheet-NH_2, sheet-cal, MCM-Au-550 and Stöber-Au-550 were 0.08, 0.21, 0.12 and 0.13 mg/mg, respectively. From these results, it was concluded that the sheet-structured samples showed high performance for IgG adsorption. In other words, sheet-Au-550 sample has comparatively higher specific surface area in sheet materials, and the surface area can effectively expose as adsorption site by the sheet characteristics. Hence MCM materials present higher specific surface area than sheet materials, however the predominantly higher proportion of interior pores makes lower accessibility to adsorbate. In addition, the presence of the AuNP on the adsorbents provided a synergistically positive effect on IgG adsorption. The effective quantity of loaded AuNPs was calculated using ICP-OES data. The amounts of Au contained in the sheet-Au-550, MCM-Au-550 and Stöber-Au-550 samples were 7.6, 8.1 and 6.7 μg/mg silica, respectively, indicating that a similar quantity of AuNPs were

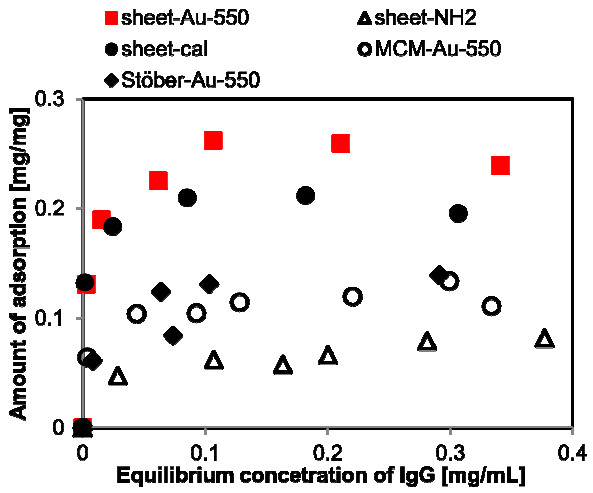

Fig. 8 Adsorption isotherms for IgG on sheet-cal, sheet-NH_2, sheet-Au-550, MCM-Au-550 and Stöber-Au-550.

loaded on each of the porous silicas. These results demonstrated that the dispersion of a small amount of gold nanoparticles can enhance IgG adsorption. However, the effect of AuNP was limited. Thus, we demonstrated that the combination of sheet-morphology for the adsorbent and the loading of dispersed AuNPs had a synergetic effect and resulted in the increased IgG adsorption capacity observed for the Au-550 sample.

Isotherm modelling and adsorption kinetics

The correlation coefficients (R^2) for the Langmuir and Freundlich models were calculated and are also listed in Table 2. The Langmuir isotherm model is based on monolayer adsorption, while the Freundlich model involves multilayer adsorption with non-uniform distribution of adsorption heats and affinities over a heterogeneous surface. The R^2 values for the Langmuir model were 0.9964, 0.9622, 0.9974, 0.9805 and 0.9693 for sheet-Au-550, sheet-NH_2, sheet-cal, MCM-Au-550 and Stöber-Au-550, respectively. Conversely, the values for the Freundlich model were found to be 0.8688, 0.8657, 0.8542, 0.8970 and 0.7753, respectively. These results clearly suggest that the Langmuir plot model gives a much better fit for IgG adsorption on all of the prepared samples than the Freundlich model. Thus, it can be concluded that IgG adsorption occurred *via* a mechanism involving typical homogenous monolayer adsorption.

Conclusions

We demonstrated the successful enhancement of antibody adsorption using dispersed AuNPs supported on an MPS sheet. The AuNPs were immobilised on an MPS sheet synthesised using TEOS and APTES as sources for the silica framework through the binding to surface aminopropyl groups acting as colloidal gold ligands. Subsequently, the loaded colloidal gold was crystallised *via* calcination at 550 °C. In all of the AuNP composites, the gold was of relatively high crystallinity. The MPS sheet exhibited an increased IgG adsorption capacity

Table 2 Maximum adsorption quantities for IgG and correlation coefficients for the Langmuir and Freundlich isotherm models.

		Langmuir	Freundlich
Carrier	Q_{Max} [mg/mg]	R^2	R^2
Sheet-Au-550	0.26	0.9964	0.8688
Sheet-NH_2	0.08	0.9622	0.8657
Sheet-cal	0.21	0.9974	0.8542
MCM-Au-550	0.12	0.9805	0.8970
Stöber-Au-550	0.13	0.9693	0.7753

compared to that of typical MCM type mesoporous silica with a similar porosity and a non-porous spherical silica. Notably, the IgG adsorption capacity was further increased by dispersing AuNPs on the MPS sheet; sheet-Au-550 had the highest Q_{Max} of 0.26 mg IgG/mg carrier. In summary, enhancement of the antibody adsorption capacity of sheet-Au-550 was due to the synergic effects of the adsorbent morphology (particularly the sheet structure) and the presence of the loaded AuNPs. Finally, the IgG equilibrium sorption data fit the Langmuir isotherm model much better than the Freundlich plot model.

Notes and references

[a] *Department of Chemistry for Materials, Graduate School of Engineering, Mie University, 1577 Kurimamachiya-cho, Tsu, Mie 514-8570, Japan. Fax: +81 59 231 9430; Tel: +81 59 231 9428; E-mail: kazuma-nakanishi@aist.go.jp*

[b] *National Institute of Advanced Industrial Science and Technology, 2266-78, Anagahora, Moriyamaku, Nagoya, Aichi 463-8560, Japan. Fax: +81 52 736 7405; Tel: +81 52 736 7551; E-mail: katsuya-kato@aist.go.jp*

1 L. R. Hirsch, J. B. Jackson, A. Lee, N. J. Halas and J. L. West, *Anal. Chem*., 2003, **75**, 2377-2381.
2 Z. S. Haidar, *Polymers*, 2010, **2**, 323-352.
3 M. P. DeLisa, Z. Zhang, M. Shiloach, S. Pilevar, C. C. Davis, J. S. Sirkis and W. E. Bentley, *Anal. Chem*., 2000, **72**, 2895-2900.
4 T. Orita, M. Tomita, K. Nakanishi and K. Kato, *J. Asian Ceram. Soc.*, 2014, **2**, 275-280.
5 F. Mi, S. Shyu, C. Chen and J. Schoung, *Biomaterials*, 1990, **20**, 1603-1612.
6 Y. Tao and G. Carta, *J. Chromatography A*, 2008, **1211**, 70-79.
7 C. Yu and J. Irudayaraj, *Anal. Chem*., 2007**, 79,** 572-579.
8 B. C. Braden and R. J. Poljak, *FASEB J*., **1995**, 9, 9-16.
9 M. Tashiro and G. T. Montelione, *Curr. Opin. Struct. Biol*., 1995, **5**, 471-481.
10 K. Nakanishi, M. Tomita, H. Nakamura and K. Kato, *J. Mater. Chem. B*, 2013, **1**, 6321-6328.
11 S. K. Bhatia, L. C. Shriver-Lake, K. J. Prior, J. H. Georger, J. M. Calvert, R. Bredehorst and F. S. Ligler, *Anal. Biochem*., 1989, **178**,408-413.
12 C. Preininger, H. Clausen-Schaumann, A. Ahluwalia and D. Rossi, *Talanta*, 2000, **52**, 921-930.
13 T. Yanagisawa, T. Shimizu, K. Kuroda and C. Kato, *Bull. Chem. Soc. Jpn.*, 1990, **63**, 988-992.
14 S. Inagaki, Y. Fukushima and K. Kuroda, *J. Chem. Soc., Chem. Commun.*, 1993, **8**, 680-682.

15 J. S. Beck, J. C. Vartuli, W. J. Roth, M. E. Leonowcz, C. T. Kresge, K. D. Schmitt, C. T. W. Chu, D. H. Olson and E. W. Sheppard, *J. Am. Chem. Soc.*, 1992, **114**, 10834-10843.
16 F. Hoffmann, M. Cornelius, J. Morell and M. Fröba, *Angew. Chem. Int. Ed.*, 2006, **45**, 3216-3251.
17 A. P. Wight and M. E. Davis, *Chem. Rev.*, 2002, **102**, 3589-3614.
18 P. Yang, S. Gai and J. Lin, *Chem. Soc. Rev*., 2012, **41**, 3679-3698.
19 H. Cai, C. Xu, P. He and Y. Fang, *J. Electroanal. Chem*., 2001, **510**, 78-85.
20 A. Doron, E. Katz and I. Willner, *Langmuir*, 1995, **11**, 1313–1317.
21 H. Chen, J. Jiang, Y. Huang, T. Deng, J. Li, G. Shen and R. Yu, *Sens. Actuators B Chem.*, 2006, **117**, 211-218.
22 Y. Fu, R. Yuan, D. Tang, Y. Chai and L. Xu, *Colloids Surf. B Biointerfaces*, 2005, **40**, 61-66.
23 N. Li, R. Yuan, Y. Chai, S. Chen, H. An and W. Li, *J. Phys. Chem. C*, 2007, **111**, 8443-8450.
24 M. Wang, L. Wang, G.Wang, X. Ji, Y. Bai, T. Li, S. Gong and J. Li, *Biosens. Bioelectron.*, 2004, **19**, 575-582.
25 C. Wang, Z. Ma, T. Wang and Z. Su, *Adv. Funct. Mater*., 2006, **16**, 1673-1678.
26 D. Pissuwan, S. M. Valenzuela, C. M. Miller and M. B. Cortie, *Nano Lett.*, 2007, **7**, 3808-3812.
27 R. M. Fratila, S. G. Mitchell, P. Pino, V. Grazu and J. M. Fuente, *Langmuir*,2014, **30**, 15057-15071.
28 K. Nakanishi, M. Tomita and K. Kato, *RSC Adv*., 2014, **4**, 4732-4735.
29 K. Nakanishi, M. Tomita and K. Kato, *J. Asian Ceram. Soc.*, in press, DOI: 10.1016/j.jascer.2014.10.011.
30 W. Yan, B. Chen, S.M. Mahurin, E.W. Hagaman, S. Dai, S.H. Overbury, *J. Phys. Chem. B*, 2004, **108**, 2793–2796.
31 M. Brust, J. Fink, D. Bethell, D. J. Schiffrin and C. Kiely, *J. Chem. Soc., Chem. Comun*., 1995, 1655-1656.
32 M. K. Corbierre, N. S. Cameron, M. Sutton, K. Laaziri and R. B. Lennox, *Langmuir*, 2005, **21**, 6063-6072.
33 M. K. Corbierre, N. S. Cameron, M. Sutton, S. G. J. Mochrie, L. B. Lurio, A. Rühm and R. B. Lennox, *J. Am. Chem. Soc*., 2001, **123**, 10411-10412.
34 M. C. Daniel and D. Astruc, *Chem. Rev*., 2004, **104**, 293–346.
35 L. M. Liz-Marzán, M. Giersig and P. Mulvaney, *Langmuir*, 1996, **12**, 4329-4335.
36 S. Cheng, Y. Wei, Q. Feng, K. Qiu, J. Pang, S. A. Jansen, R. Yin and K. Ong, *Chem. Mater*., 2003, **15**, 1560-1566.
37 Y. Jin, P. Wang, D.Yin, J Liu, H. Qiu, N. Yu, *Micropor. Mesopor. Mat*., 2008, **111**, 569-576.
38 B. Lee, Z. Ma, Z. Zhang, C. Park and S. Dai, *Micropor. Mesopor. Mat*., 2009, **122**, 160-167.
39 B. Lee, H. Zhu, Z. Zhang, S. H. Overbury and S. Dai, *Micropor. Mesopor. Mat*., 2004, **70**, 71-80.
40 K. Kambara, N. Shimura and M. Ogawa, *J. Ceram. Soc. Jpn*., 2007, **115**, 315-318.
41 M. Bradford, *Anal. Biochem*., 1976, **72**, 248-254.